Wind-driven rivulet over an edge with break-up

Tobias Tivert*, Andreas Borg†, Jose Marimon* and Lars Davidson*

Chalmers University of Technology

Dept. of Applied Mechanics, Division of Fluid Dynamics

SE-412 96 Gothenburg, Sweden

tobias.tivert@chalmers.se

Keywords:Rivulet, Breakup, VOF, Experiment

Abstract

An experimental and numerical study of a wind-driven rivulet break-up at the trailing edge of a horizontal plate was carried out. The experiment setup is a $20mm$ thick, $260 \times 300mm^2$ plate with a $1mm$ circular water inlet centered on top of the plate. The ambient air flows on both sides of the plate. As the water is introduced, the ambient air will form a rivulet that travels towards the trailing edge of the plate. The rivulet breaks-up, at the trailing edge forming droplets with sizes that depend on the flow rate and velocity of the ambient flow.

The experimental part was done at Volvo Car Corporation using three different water flow rates (0.8, 0.5 and $0.2l/h$) and four ambient air flow velocities (11, 14, 19 and $25m/s$). A high-speed camera was used to visualize the water which contained a flourecent liquid for easier post-processing. Every case was repeated ten times in order to obtain reasonably good statistics for the pinch-off frequency and the second order droplets. The static contact angle and surface tension were also measured.

Numerical simulations were carried out using the numerical method volume of fluid (VOF) within the commercial software FLUENT. The cases simulated were the experimental cases having the largest experimental water flow rate. This choice was based on earlier numerical generic studies of rivulets. It was concluded that a low water flow rate did not predict a rivulet, but a droplet train, on the plate in contrast to experiments.

The computational domain was discretized using a block-structured boundary-fitted mesh. The choice of hexahedral mesh was based on previous experience that showed poor performance of the VOF method on tetrahedral/prismatic mesh structures when there are strong gradients in the prismatic layer. The air flow is calculated without a turbulence model. The boundary layer is laminar upstream of the water inlet and matches the Blasius profile.

The simulations show fairly good agreement with experiments in terms of droplet sizes and velocity, but it under predicts the results a little bit. This is probably because the rivulet arrives at the trailing edge with too high velocity and does not want to stay at the lower edge long enough to accumulate large droplets. This is because the model does not include surface roughness and dynamic contact angle.

Introduction

Modeling the soiling of side windows caused by the side rear view mirrors is of great importance in the car industry. The reason is that the soiling of the side windows diminishes the driver's view of the mirror. Simulations must be made of various test cases to simulate the water behavior on a side rear view mirror. The numerical methods and the physical models working on the scales of interest must be validated.

The test case studied in the present work is a wind-driven rivulet on a horizontal plate with break-up at the trailing edge. It is a suitable case since it involves much of the physics and difficulties present in a simulation on a rear view side mirror.

Three different water flowrates and four different air flow speeds, were used in the experimental part.

The experimental study was done to try to understand more about the droplet break up process and to support the CFD simulations.

Only the case of the highest water flow rate and the lowest wind speed was simulated, in the CFD calculation.

Nomenclature

VOF	volume of fluid
P	pressure
DCA	dynamic contact angle
UD	upwind differencing
DD	downwind differencing
S	mass source term
Co	Courant number
CSF	continuum surface force
HRIC	high resolution interface capturing

Greek letters

α	volume fraction
μ	viscosity
σ	surface tension
ρ	density

Experimental Study

The main interest in the experiment was to register the radius and velocity of the released droplets at different distances from the trailing edge. Schematic pictures of the experiment dimensions are presented in Fig. 1 and Fig. 2.

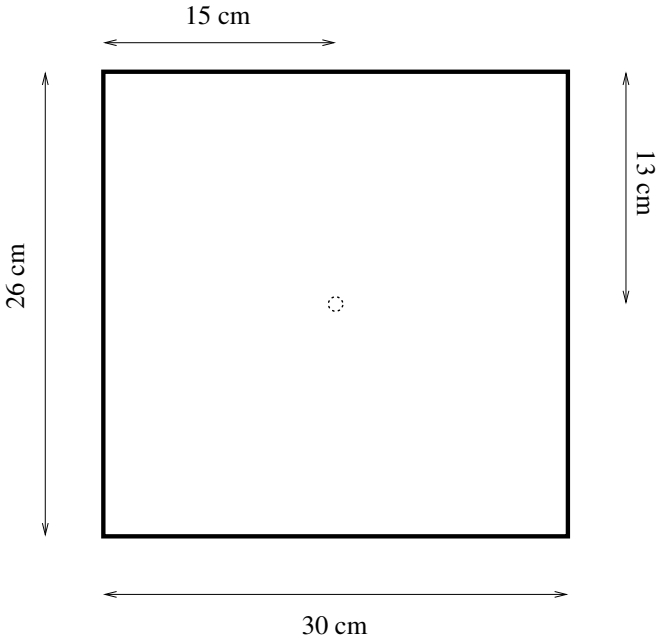

Figure 1: Plate from above

The static contact angle was also measured. The experimental equipment was a high-speed camera with a resolution of 256×256. A still picture camera was also used with a resolution of 9M pixels, this was mainly used when the rivulet (droplet) was stationary. The first measurement made was of the static contact angle. Figures 3 and 4 present photos taken at two different locations on the plate for different liquids.

The analysis of the contact angles was carried out in photoshop and the values are given in Table 1.

The velocity and size of the released droplets were obtained by high-speed filming UV-liquid was used in order to obtain sharper pictures. The pictures were analyzed in Matlab with a imagetoolbox where the movement of each centroid was detected. The velocities of the droplets were obtained from the camera frequency. The measurements were repeated ten times for each waterflow rate and ambient air flow to obtain good statistics. The duration of each film was two seconds with a frequency of 1000 Hz. A typical picture from the high-speed camera is shown in Fig. 5.

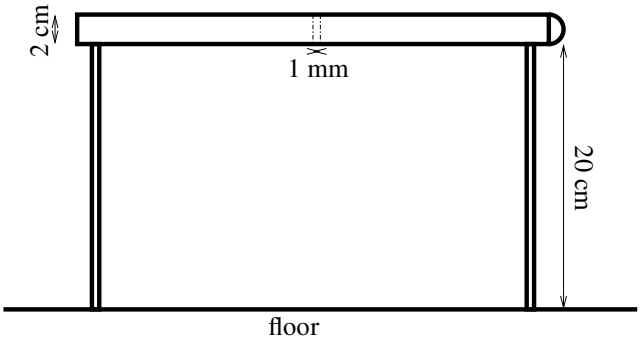

Figure 2: Plate from side

Figure 4: Measurement of the static contact angle.

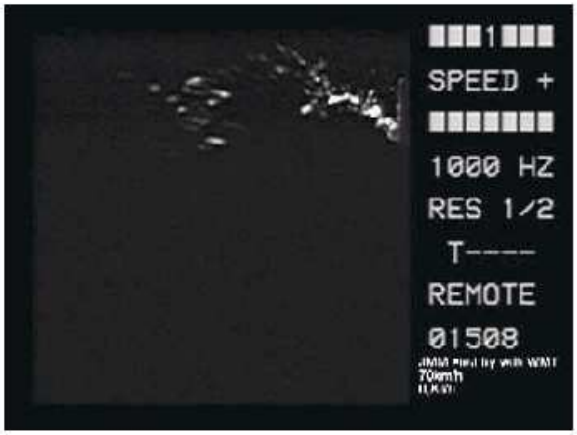

Figure 5: One frame from the high-speed camera. The white area is water.

The experiments error such as blurriness and converting between different formats has been corrected for. Greater detail on the experimental work is given in Lafuente (2007).

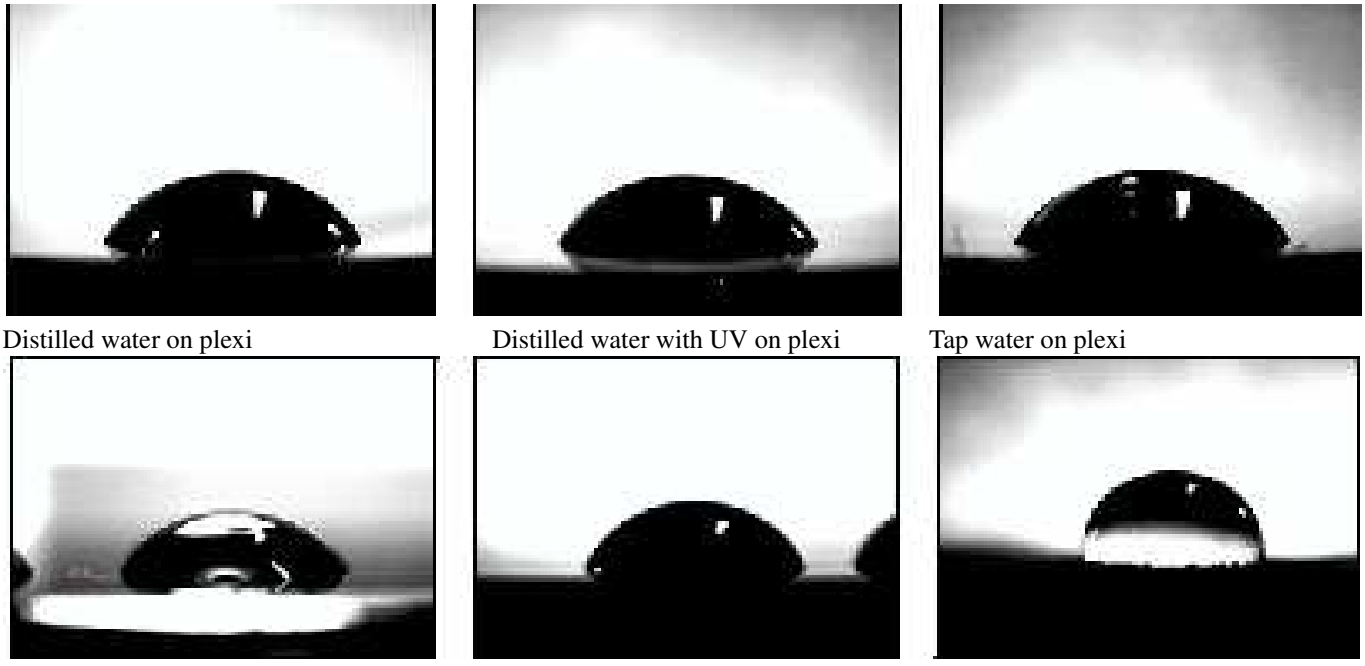

Distilled water on plexi | Distilled water with UV on plexi | Tap water on plexi

Distilled water on mirror | Distilled water with UV on mirror | Tap water on wax

Figure 3: Static contact angle of different liquids and solids.

	Specimen left (degrees	Contact angle right (degrees)	Mean (degrees)	Estimated error	Relative error
Distilled water on mirror	57.6	62			
Distilled water on mirror2	59	64.8	61	8	0.13
Distilled water and UV on mirror	57.6	62			
Distilled water on mirror2	59	64.8	61	8	0.13
Distilled water on plexi	60.4	61.4			
Distilled water on plexi2	58	59.7	60	8	0.13
Distilled water on and UV plexi	59.8	56.7			
Distilled water on and UV plexi2	61.5	62.7	57	8	0.13
tap water plexi	58.3	60.1			
tap water plexi2	55.3	54.8	60	8	0.13

Table 1: Contact angles for some combination of liquids and solid.

Theory

VOF

A multiphase model is needed to simulate a flow with two or more different fluids. It can be either Lagrangian particle tracking, Euler-Euler, VOF (Volume of fluid) or something similar. In our case VOF is suitable, since we are interested only in the location of the interface between the water and air. The equations are fairly simple. One set of momentum and continuity equations and an interface tracking equation, which is simply a convection equation are solved. The equations are given as

$$\begin{aligned} \frac{\partial}{\partial t}\rho u_i + \frac{\partial}{\partial x_j}(\rho u_i u_j) &= -\frac{\partial p}{\partial x_i} \\ + \frac{\partial}{\partial x_j}\left[\mu\left(\frac{\partial u_i}{\partial x_j} + \frac{\partial u_j}{\partial x_i}\right)\right] &+ \rho g_i + F_i \qquad (1) \\ \frac{\partial u_j}{\partial x_j} &= 0 \end{aligned}$$

The fluid properties are calculated as

$$\begin{aligned} \rho &= \alpha_2\rho_2 + \alpha_1\rho_1 \\ \mu &= \alpha_2\mu_2 + \alpha_1\mu_1 \end{aligned} \qquad (2)$$

where α is an indicator function that identifies which of the fluids is in the cell.

$\alpha_i = 0$ if the cell is empty of fluid i

$\alpha_i = 1$ if the cell is full of fluid i

$0 < \alpha_i < 1$ if the cell contains both fluids

and the relation for the indicator functions must fulfil

$$\sum_{i=1}^{2} \alpha_i = 1 \qquad (3)$$

Since there are only two phases in the present application (water and air), we need only solve for one indicator, α. The

indicator function equation is simply a scalar transport equation for the interface.

$$\frac{\partial \alpha}{\partial t} + \frac{\partial \alpha u_i}{\partial x_i} = 0 \tag{4}$$

Term F_i in the momentum equation denotes surface tension. FLUENT uses the CFS of Brackbill et al. (2006) for the calculation of surface tension and the term has the form

$$F_i = -(\sigma \bigtriangledown \alpha) \bigtriangledown \cdot \left(\frac{\bigtriangledown \alpha}{| \bigtriangledown \alpha |} \right) \tag{5}$$

This term is very large at the interfaces, which is the main reason why VOF simulations are numerically very unstable. An accurate solution requires sharp interfaces, but unfortunately the sharp interfaces make the surface tension term very large, which in turn makes the equations numerically unstable. Hence we cannot afford interfaces that are too sharp. The equations stay reasonably stable for droplet sizes down to a couple of centimeters, but they become very unstable for droplet sizes of a couple of millimeters. In this work we have tried to reach a compromise: we use a discretization scheme for the α equation that is fairly stable. The drawback is that the scheme is not as sharp as Young's scheme.

HRIC

The modified HRIC scheme that consists of a non-linear blending of upwind and downwind differencing was developed by Muzaferiju and Peric (2000). Pure upwind will be bounded but is too diffusive. Downwind is unstable but not diffusive so the combination is suitable for VOF calculations. First the normalized volume fraction $\overline{\alpha}$ in the cell center is computed as

$$\overline{\alpha} = \frac{\alpha - \alpha_u}{\alpha_d - \alpha_u} \tag{6}$$

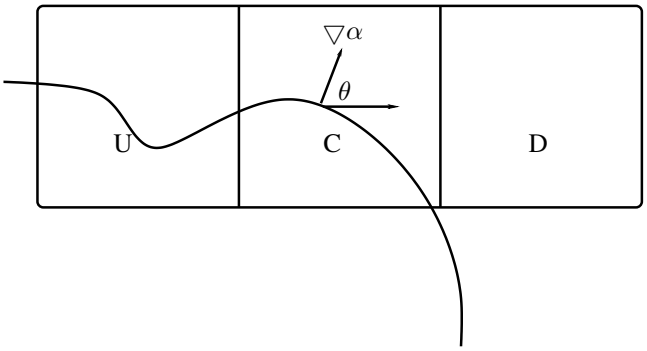

Figure 6: The HRIC discretization scheme

Subscripts U, D and C in Fig. 6 denote upstream, downstream and the actual cell, respectively. With $0 < \alpha < 1$, the face value of α is computed as

$$\alpha_f = \begin{cases} \alpha_c & \text{if } \alpha_c < 0 \\ 1 & \text{if } 0.5 < \alpha_c < 1 \\ \alpha_c & \text{if } 1 < \alpha_c \end{cases}$$

Direct use of α_f can cause wiggles at the interface if the flow is parallel to the interface. To prevent this the HRIC

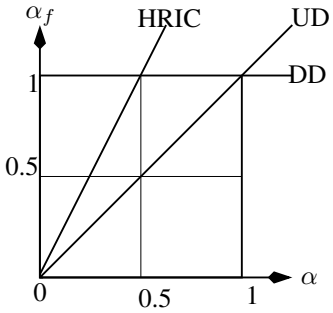

Figure 7: cell

scheme uses the angle between the interface and the normal vector to the grid face. α_f is corrected as

$$\alpha_f^* = \alpha_f \sqrt{cos\theta} + \alpha_f (1 - cos\theta)$$

If the local Courant number ,Co, is too large, convergence problems may be encountered. HRIC also takes into account high local Co, and thus the face value of α_f is corrected as

$$\alpha_f^{**} = \begin{cases} \alpha_f^* & \text{if } Co < 0.3 \\ \alpha_c & \text{if } 0.7 < C_o \\ \alpha_c + (\alpha_f^* - \alpha_c)\frac{0.7 - Co}{0.4} & \text{otherwise} \end{cases}$$

Here, Co is defined as

$$Co = \frac{v \cdot n S_f \Delta t}{V_f}$$

Finally we obtain the HRIC scheme

$$\alpha_f = \gamma \alpha_c + (1 - \gamma)\alpha_D$$

where γ is defined as

$$\gamma = \frac{(1 - \alpha_f^* *)(\alpha_D - \alpha_U)}{\alpha_D - \alpha_c}$$

The HRIC scheme is available in Fluent.

Domain

The computational domain has dimensions $21 \times 400 \times 80mm^3$. It was necessary to include the entire plate in the computational domain in order to correctly predict the boundary layer growth. The width of the plate has been reduced, and thus the computational domain extends one centimeter at each side of the hole (the diameter of the hole is one millimeter). The reduction of the computational domain is not expected to have any effect on the predicted results.

Boundary conditions

Symmetry boundary conditions are applied in the spanwise boundaries (low and high x) and at the bottom and top (low and high z). The air speed is set to $11.1m/s$ at the inlet (low y). The speed of the water through the hole in the middle of the plate is set to $0.23m/s$. Neumann boundary conditions are prescribed at the outlet. The static contact angle is set to 60^o.

Grid

The grid that was used consists of 4.4 million cells. The quality of the mesh was perfect since a pure hexahedral mesh was used. A finer mesh was used at the expected location of the rivulet. The first node is set in the "linear layer" of the Blasius profile and consequently this node is located approximately $0.3mm$ from the wall see Fig. 8. However since our earlier work indicated that a rivulet must be resolved by at least four cells, the first cell is located at $0.2mm$ from the wall.

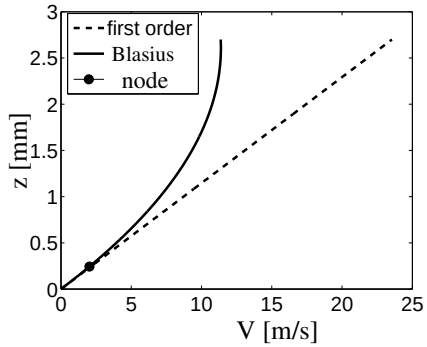

Figure 8: First node in the "linear layer"

The cells are $0.2 \times 0.2mm^2$ in the $x - z$ plane in a box that extends the entire domain in the y direction, and the box is $8 \times 8mm^2$. Outside the box the grid is stretched by 3% in the (x) and (z) direction. The grid in the streamwise direction (y) is stretched from the hole to the inlet by 4%.The grid spacing is constant from the hole to the edge, and downstream of the edge 1% streaching is used. A typical snapshot of the velocity field is shown in Fig. 9.

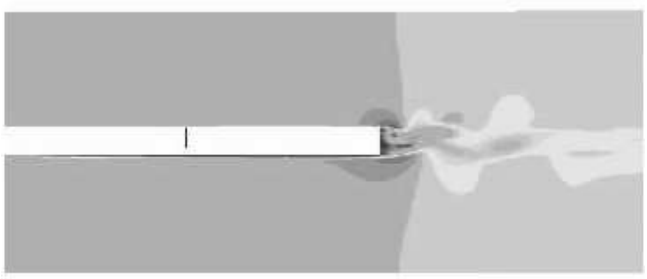

Figure 9: Snap shot of the velocity field. Flow from right to left.

The V velocities along the upper of the plate are shown in Fig. 10 and, as can be seen, they agree well with the Blasius profiles.

Results and Discussion

In our previous investigation of the gravity-driven rivulet simulations we found that the predicted break-up of the the rivulet took place too early as compared to experiments. We thus decided in the present work to simulate the highest water flow rate and the lowest air velocity. It turns out that the rivulet breaks up in this case as well. This may be a resolution problem. The fine grid (cells of $0.1mm$; the baseline grid has cells of $0.2mm$) shows better tendencies, but it was

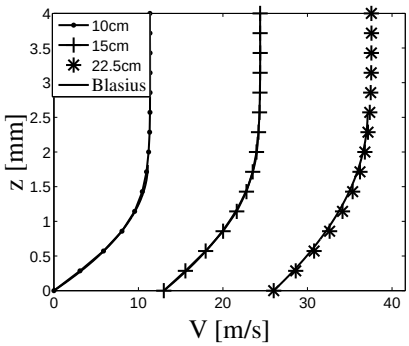

Figure 10: Computed and analytic laminar boundary layer at different distances from the inlet.

impossible to obtain a converged solution even when 40 iterations per time step and a Co number of 0.2 were used. One reason is that the rivulet moves too fast. The only force that breaks up the rivulet in the simulation is the shear stress between the water and the solid wall. In reality, many more physical processes come into play, such as the difference in contact angle, wetting properties, roughness etc. In the case of a droplet the dynamic contact angle (DCA) has great importance for the velocity, but it will not have that great impact on the speed in the case of a rivulet. The pressure difference over a droplet is caused by the difference in surface curvature at the back and front sides. A rivulet has only a front side, and no back side, and hence the effect of increasing the dynamic contact angle is similar to that of increasing the static contact angle.

Several modifications were tested to prevent break-up of the rivulet.

1. First, the initial boundary conditions were modified so that the rivulet was defined at the plate at time zero. This did not help, and the rivulet broke up anyway , it simply took place somewhat later.

2. Second, we increased the wall shear stress of the rivulet to decrease its speed. The physical argument was that we introduced surface roughness of the wall by increasing the viscosity. The lowest viscosity at which the rivulet did not break up was six times the physical viscosity. One advantage in modifying the viscosity is that the Weber number, which governs the break up, does not change. We believe that increasing the viscosity does not have any large negative effect since the VOF model, even when using the physical viscosity, over-predicts the speed of the rivulet.

3. Third, we moved the hole closer to the trailing edge using the physical viscosity. The hole was placed one centimeter from the edge. In this way, the rivulet does not break up.

We decided to run the simulations with a hole close to the edge (the third alternative above) because we are primarily interested in the break-up process. A break-up upstream of the edge would most likely affect the frequency of the rip-off at the lower corner of the edge. The rip-off frequency would

probably be governed by the frequency of the rivulet break-up on the plate, and that would affect the size of the droplets leaving the lower corner of the edge.

Figure 11: A rivulet with physical viscosity, μ

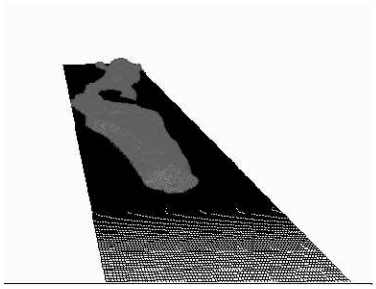

Figure 12: Unstable rivulet with fine mesh (cells of $0.1mm$)

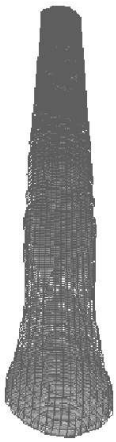

Figure 13: A rivulet with viscosity 6μ

Figure 11 illustrates that the rivulet breaks up if no modification is used. When the viscosity is increased by a factor of six (Fig. 13), the rivulet does not break up. Figure 12 shows that, when using a finer mesh than the baseline mesh, the rivulet breaks-up later but becomes unstable. It is not clear whether this behaviour is physically realistic or not.

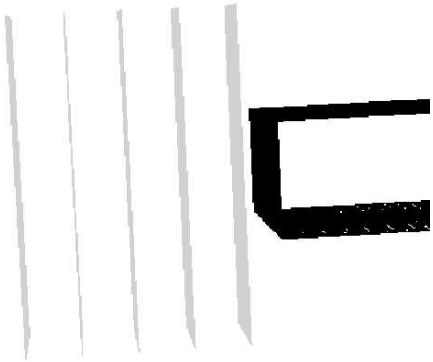

Figure 14: Planes with constant y for storing data.

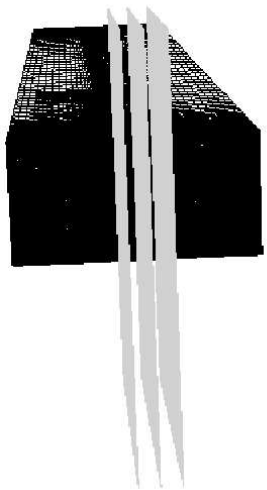

Figure 15: Planes with constant x for storing data.

Data storage

Instantaneous data must be stored to trace the droplets that are being ripped off at the lower corner of the edge. Due to space limitations we could not store the complete set of data, and thus a couple of planes were chosen. Five planes with constant x were chosen downstream of the edge separated by $5mm$, see Figure 14; the first plane is located $5mm$ downstream of the edge. Another three planes with constant y were selected, see Fig. 15, which are separated by $3mm$; the first plane is located at the symmetry plane.

A snapshot series of a droplet moving in the center plane is shown in Figs. 16-21. Figure 16 shows how the ambient flow begins to rip off the droplet from the lower corner of the edge. $9ms$ later, the droplet starts to release from the corner, Figure 17. Figure 18 shows how the droplet at the lower edge is released and how a new droplet begins to form at the upper corner. The shape of the droplet that is released is elongated. In Fig. 19 the shape of the droplet has became fairly circular. Figure 20 shows how the droplet starts to break up.

Figure 16: Time $t = t_1$.

Figure 17: Time $t = t_1 + 9ms$.

Figure 18: Time $t = t_1 + 12m$.

Figure 19: Time $t = t_1 + 15ms$.

Figure 20: Time $t = t_1 + 18ms$.

Figure 21: Time $t = t_1 + 21ms$.

Unfortunately, it does not take place in the center plane, and we therefore cannot visualize it to any great degree with our stored instantaneous data. Figure 21 shows the droplet when it has reached its final size; it will not break up any further. It has been two or three satellites that not are in the center plane.

Velocity and radius calculation

This sub-section gives an evaluation of the predicted speed and computationally size of the droplets. To locate a droplet in the domain we need to find a closed area. It is computationally very expensive to do this on an unstructured grid (FLUENT is an unstructured solver). Hence we do it in the following way.

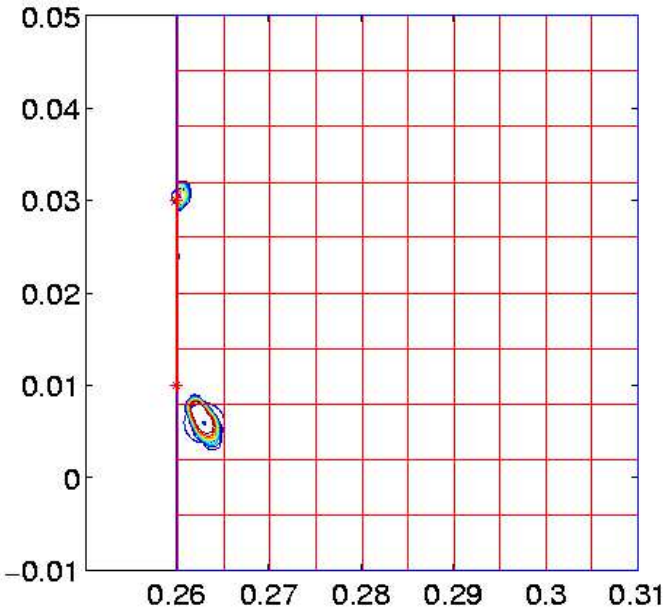

Figure 22: The seek algorithm, the search mesh and a droplet with its corresponding radius

Step 1: Interpolate the data to a Cartesian grid with second order accuracy.

Step 2: Define a very coarse grid (see Fig. 22) where each cell is checked to see whether it contains any volume fraction.

Step3: If there is any volume fraction in the large cell, then an algorithm must find the closed area.

Step 4: If a droplet is in two or more cells then a new large cell is defined. It is not a problem if we have more than one droplet in a cell.

Step 5: Compute a corresponding radius of the closed area.

Step 6: Compute the distance between the droplets and divide it by the time step, which gives the speed of the droplet.

The approach described above is carried out in Matlab.

Comparison with experiment

Figures 23 and 24 present the predicted and the measured radii and velocities of the droplets. The measured data have been averaged over many droplets. We accumulated predicted data that cover the release of three droplets. Hence the predicted results in Figs. 23 and 24 are presented as scatter plots which cover the three droplets at all time steps.

The predicted radii are somewhat lower than the experimental values. The result is that the velocities of the droplets are over-predicted, since a small droplet accelerates faster than a large one. The discrepancy between predictions and experiments is probably due to the too high velocity of the rivulet. This gives too small accumulation of water before it rips off.

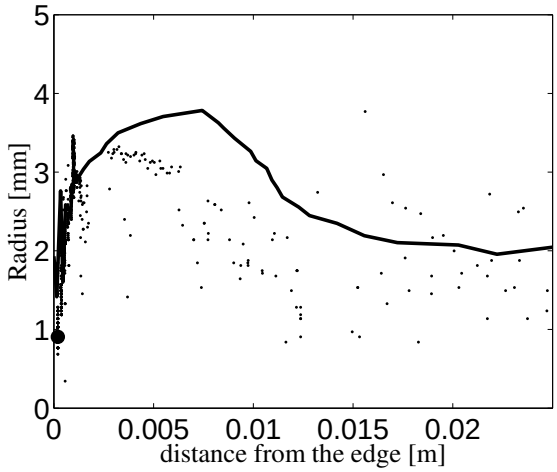

Figure 23: Radius of the droplets. Dots: predictions; solid line: experimental data.

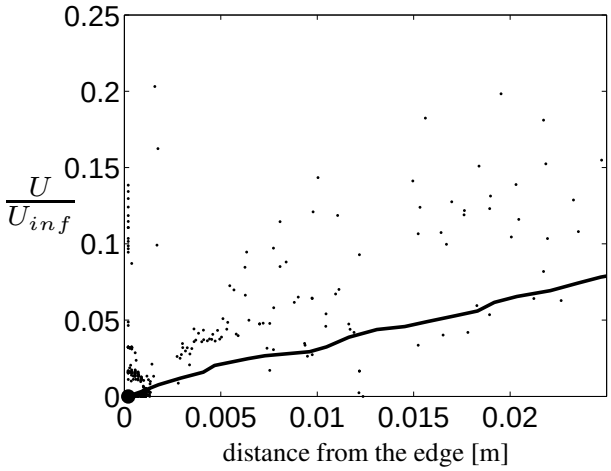

Figure 24: Velocity magnitude of the droplets. Dots: predictions; solid line: experimental data.

The predicted data at the left hand side of the plots represent droplets that are moving downwards along the vertical edge. It appears as though they are over-represented, but the reason is that they are detected at each time step. The releasing frequency in the experiment was $1.619Hz$ and in the simulation $2.04Hz$. This discrepancy illustrates the same problem as before: the predicted velocity of the rivulet is too high.

Conclusions

This work has reported the results of a wind driven rivulet on a flat plate for a water flow rate $0.8l/h$ and an air flow of $11.11m/s$. CFD predictions have been compared with experimental data.

To prevent the rivulet from break-up before it reached the plate edge, the release hole location had to be modified using the current model.

The simulations show fairly good agreement with experimental results in terms of droplet size and droplet velocity.

Future work

The method of using a plane for the date storage works fairly well, but not perfectly. In the next simulation a bounded box should replace the plane. The box will be placed such that we can capture all the droplets and extend from the edge and 3.5 cm downstream. It is not necessary for it to be bigger because, after 3.5 cm, the results are too diffuse because of the mesh and the scheme. Other air velocities will also be tested, especially 19 and 25 m/s.

Acknowledgements

This project is financed by Vinnova and the Volvo Car Corporation. We would like to thank the Volvo Car Corporation for support with the wind tunnel and experimental materials.

References

J.U Brackbill, D. B. Kothe, and C. Zemach. A continuum method for modeling surface tension. *Journal of Computational Physics*, 100:335–354, 2006.

Fluent. Fluent 6.3 users guide, fluent inc. , 2006.

José M.M Lafuente. Experimental studies of water management on a flat plate and simplified rear view mirror. MSc Thesis 07/15, Division of Fluid Dynamics, Departmwent of Applied Mechanics, Chalmers University of Technology, Göteborg, Sweden, 2007.

S. Muzaferiju and M. Peric. A two-fluid Navier-Stokes solver to simulate water entry. In *22nd Symposium on Naval Hydrodynamics*, pages 638–651, 2000.